Chapter 10

A Thermodynamic Investigation of Adsorbate-Adsorbate Interactions of Carbon Dioxide on Nanostructured Carbons

M. Murialdo, C.C. Ahn, and B. Fultz, "A Thermodynamic Investigation of Adsorbate-Adsorbate Interactions of Carbon Dioxide on Nanostructured Carbons," AIChE J. (submitted, 2016).

Abstract

A thermodynamic study of carbon dioxide adsorption on a zeolite-templated carbon (ZTC), a superactivated carbon (MSC-30), and an activated carbon (CNS-201) was carried out at temperatures from 240 to 478 K and pressures up to 5.5 MPa. Excess adsorption isotherms were fitted with generalized Langmuir-type equations, allowing the isosteric heats of adsorption and adsorbed-phase heat capacities to be obtained as a function of absolute adsorption. On MSC-30, a superactivated carbon, the isosteric heat of carbon dioxide adsorption *increases* with occupancy from 19 to 21 kJ□ mol^{-1}, before decreasing at high loading. This increase is attributed to attractive adsorbate-adsorbate intermolecular interactions as evidenced by the slope and magnitude of the increase in isosteric heat and the adsorbed-phase heat capacities. An analysis of carbon dioxide adsorption on ZTC indicates a high degree of binding-site homogeneity. A generalized Law of Corresponding States analysis indicates lower carbon dioxide adsorption than expected.

1. Introduction

Anthropogenic contributions to carbon dioxide in the atmosphere have become an ever-increasing concern, recently highlighted by the IPCC Fifth Assessment Report[1]. Given the growing nature of world energy demands and our continued reliance on fossil fuels, carbon-capture and storage (CCS) should be considered in any plan to mitigate climate change.[2,3]

Physisorptive materials are promising for a variety of gas applications because they require only low regeneration energies and are stable through thousands of cycles.[4,5] In physisorption, solid adsorbents induce a local densification of gas at the adsorbent surface by weak physical interactions. Physisorptive materials have been widely used for gas storage applications. [6,7] Because different gases adsorb to a given surface with differing selectivities, physisorptive materials are also promising for gas separations[8,9]. A number of studies have shown that physisorptive materials are viable candidates for separating carbon dioxide from mixed-gas streams.[10,11,12]

An adsorbent's selectivity of one gas over another is dependent on the thermodynamic properties of the gas-adsorbent system. As gas molecules are adsorbed, their molar entropy decreases. This is offset by a decrease in molar enthalpy from favorable interactions between the adsorbate and the adsorbent. The differential change in molar enthalpy at constant surface occupancy, defined as the isosteric enthalpy of adsorption (ΔH_{ads}), is an important and readily accessible figure of merit for physisorptive processes.[13] Optimizing the isosteric enthalpy of adsorption has been the topic of active research.[14,15,16] A variety of high surface area materials including metal-organic frameworks, covalent-organic frameworks, zeolites, zeolite-templated

carbons, and activated carbons have been investigated as carbon dioxide adsorbents, and have exhibited isosteric heats of adsorption of up to 90 kJ•mol^{-1} .[17,18,19,20,21,22,23]

In general the isosteric heat of adsorption ($-\Delta H_{ads}$) decreases as a function of surface loading due to heterogeneity of the binding sites.[24] This has the effect of limiting the pressure range over which gas separation and storage are optimal. However, recent investigations of nonideal gases adsorbed on carbonaceous materials at high pressures have shown that, in some systems, strong lateral intermolecular interactions between adsorbate molecules can lead to an isosteric heat of adsorption that increases with increasing occupancy near ambient temperatures.[25,26,27,28] This effect is realized in adsorbent materials with optimal surface structure and a narrow distribution of binding-site energies.[29,30] At high pressures, carbon dioxide gas has strong intermolecular interactions and nonideal behavior, and is therefore a candidate for this effect. In this paper we report that the superactivated carbon MSC-30 has an atypical, increasing isosteric heat of carbon dioxide adsorption, and we provide evidence that this effect derives from adsorbate-adsorbate intermolecular interactions.

2. Experimental Methods

Carbon dioxide uptake was measured on three carbonaceous materials: CNS-201, MSC-30, and ZTC. The activated carbon CNS-201 was obtained from A.C. Carbons Canada Inc., and MSC-30, a superactivated carbon, was obtained from Kansai Coke & Chemicals Company Ltd. ZTC was synthesized by infiltrating zeolite NaY with furfuryl alcohol followed by polymerization, carbonization and the ultimate dissolution of the zeolite template. This synthesis has been described in detail elsewhere[31]. Each material was degassed at 520 K under

vacuum (less than 10^{-3} Pa) prior to measurements. The skeletal densities of the materials were determined by helium pycnometry.

Equilibrium N_2 adsorption isotherms were measured at 77 K with a BELSORP-max volumetric instrument (BEL-Japan Inc.), and surface areas were calculated using the Brunauer-Emmett-Teller (BET) method[32]. The Dubinin-Radushkevich (DR) method[33,34] was used to calculate micropore volumes. Pore-size distributions were calculated by the non-local density functional theory (NLDFT) method[35] from high-resolution data collected on a Micromeritics ASAP 2020, using a carbon slit-pore model and software provided by Micromeritics.

Equilibrium carbon dioxide adsorption isotherms were measured at up to nine temperatures between 240 and 478 K using a custom Sieverts apparatus that was designed and tested for accuracy to 10 MPa[36]. The sample holder was submerged in an isothermal chiller bath for low temperature isotherms, or placed inside a cylindrical copper heat exchanger and wrapped with insulated fiberglass heating tape for high temperature isotherms. A proportional-integral-derivative (PID) controller was used to maintain a constant temperature during measurements; fluctuations were less than ± 0.1 K at low temperatures and no higher than ± 0.4 K at high temperatures.

The Sieverts apparatus is equipped with a digital cold cathode pressure sensor (I-MAG, Series 423) and a molecular drag pump capable of achieving a vacuum pressure of 10^{-4} Pa. High-pressure measurements were made using an MKS Baratron (Model 833) pressure transducer. Temperature was measured on the wall of the manifold and on the outer wall of the sample holder using K-type thermocouples and platinum resistance thermometers. Supercritical fluid chromatography (SFC) grade carbon dioxide (99.995%) gas was obtained from Air Liquide America Corporation, and multiple adsorption/desorption isotherms were

measured to ensure reversibility and reproducibility. Gas densities were determined from the REFPROP Standard Reference Database[37].

3. Results

3.1. Nitrogen Adsorption and Helium Pycnometry

The pore-size distributions calculated by nonlocal density functional methods of CNS-201, MSC-30, and ZTC are shown in Figure 1. CNS-201 was found to have distinct, extremely narrow pore sizes of < 1.5 nm in width. MSC-30, on the other hand, has a broad pore size distribution with pore widths ranging from 0.6 to >3 nm. ZTC has a single dominant pore width of 1.2 nm, consistent with the inverse of the zeolite structure. The BET surface areas of MSC-30, CNS-201, and ZTC were found to be 3244±28, 1095±8, and 3591±60 $m^2 \bullet g^{-1}$, respectively. ZTC is one of the highest specific surface area carbonaceous materials reported to date. The micropore volumes of MSC-30, CNS-201, and ZTC were determined to be 1.54, 0.45, and 1.66 $mL \bullet g^{-1}$, respectively. The theoretical maximum possible carbon dioxide adsorption (n_m) was estimated as the product of the micropore volume and the density of liquid carbon dioxide at its triple point,[30] yielding estimated n_m values of 41.3, 12, and 44.5 $mmol \bullet g^{-1}$ for MSC-30, CNS-201, and ZTC, respectively. MSC-30 and CNS-201 have skeletal densities of 2.1 $g \bullet mL^{-1}$, while ZTC has a lower skeletal density of 1.8 $g \bullet mL^{-1}$ due to a higher hydrogen content[38].

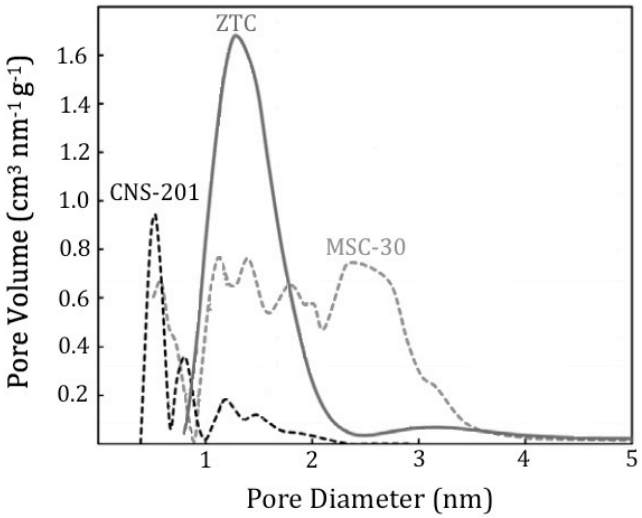

Figure 1. The pore-size distribution of MSC-30, CNS-201, and ZTC as calculated by the NLDFT method.

3.2. Carbon Dioxide Adsorption

Equilibrium excess adsorption isotherms of carbon dioxide on the nanostructured carbons are shown in Figure 2. The low temperature isotherms display maxima at pressures between 0.5-5 MPa, as expected for Gibbs excess quantities. At all measured temperatures, MSC-30 has the highest maximum excess adsorption quantities. At room temperature (298 K), the maximum excess uptakes on MSC-30, CNS-201, and ZTC were 22.7, 7.25, and 17.8 mmol•g^{-1} respectively, corresponding to 7.00, 6.62, and 4.96 mmol•(1000 m^2) $^{-1}$. This correlation of BET surface area and Gibbs surface excess uptake maximum capacity is consistent with other similar materials, which have an average "Chahine's-type rule" for carbon dioxide uptake at 298 K of ~7 mmol (1000 m^2) $^{-1}$ [39].

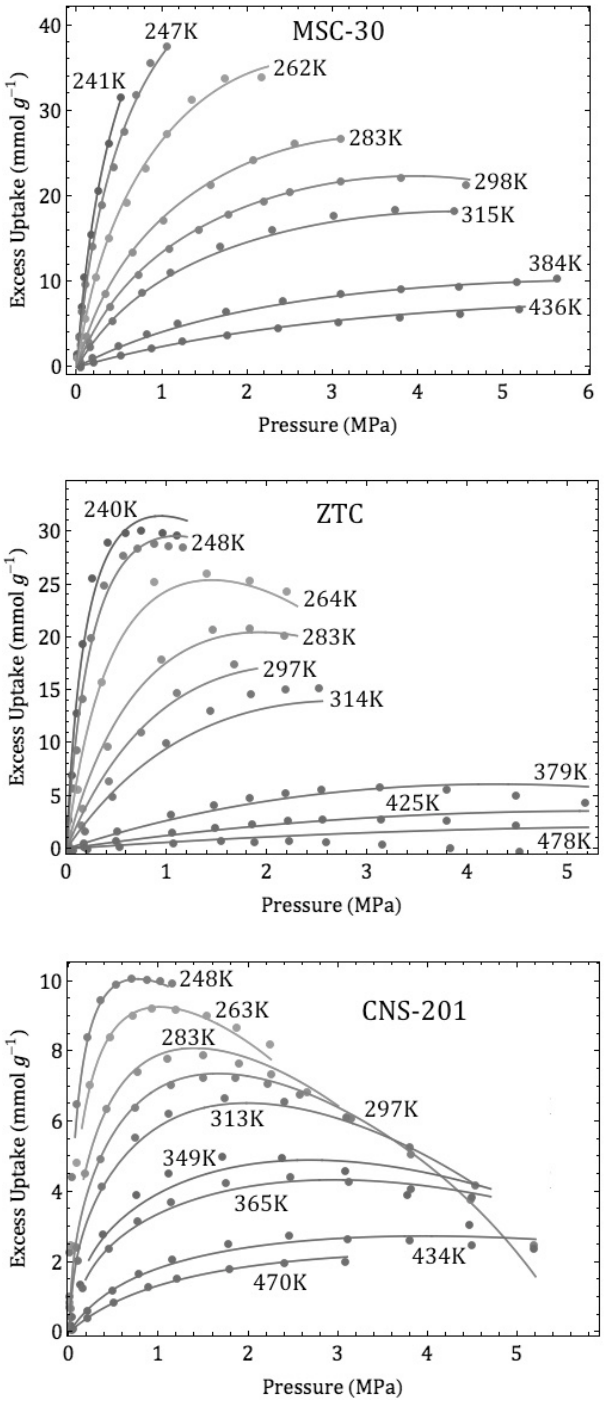

Figure 2. Equilibrium excess adsorption isotherms of carbon dioxide on MSC-30 (top), ZTC (middle), and CNS-201 (bottom). The curves show the best simultaneous fit of the measured data for a given material, using Equation 2 below.

3.3. Adsorption Data Analysis

Adsorption measurements give excess adsorption (n_e), not absolute adsorption (n_a).[40] At low pressures, excess adsorption approximates absolute adsorption. At high pressures, however, the absolute adsorption remains a monotonically increasing quantity, but excess adsorption does not. By utilizing a fitting equation consistent with the definition of excess adsorption, measured data can be fitted beyond the maximum of excess adsorption. Our carbon dioxide excess adsorption isotherms were fitted using a generalized Langmuir equation, recently described and applied to high-pressure methane adsorption.[29] This fitting technique was adapted from that implemented by Mertens[41].

The fitting procedure incorporates the Gibbs definition of excess adsorption, which is related to absolute adsorption as follows:

$$n_e = n_a - V_a\rho(P,T) \quad (1)$$

The gas density (ρ) is a function of pressure (P) and temperature (T) and was estimated from the modified Benedict–Webb–Rubin equation of state[37]. The volume of the adsorption layer, V_a, is the only unknown preventing direct calculation of absolute adsorption. Here V_a, is left as an independent fitting parameter. The Gibbs excess adsorption was fitted using the following generalized Langmuir equation:

$$n_e(P,T) = (n_{max} - V_{max}\rho(P,T))\left[\sum_i \alpha_i \frac{K_iP}{1+K_iP}\right] \quad (2)$$

$$K_i = \frac{A_i}{\sqrt{T}} e^{-E_i/RT} \quad (3)$$

$$\sum_i \alpha_i = 1 \quad (4)$$

The independent fitting parameters are α_i (weighting factors) and K_i (equilibrium constants) for the i Langmuir isotherms, the scaling factor n_{max}, and the maximum volume of the

adsorption layer V_{max}. The equilibrium constants (Equation 3) depend on the prefactors (A_i) and energies (E_i) of the Arrhenius-type exponentials and R, the universal gas constant. For a good balance between number of fitting parameters and goodness of fit, the number of superimposed Langmuir equations used was i=2. The residual mean square values of the resulting fits of the adsorption data for MSC-30, CNS-201, and ZTC were 0.1, 0.07, and 0.7 $(\text{mmol g}^{-1})^2$ respectively.

The best-fit parameters of carbon dioxide on MSC-30, CNS-201, and ZTC are compared to the best-fit parameters of methane[25], ethane[26], and krypton[27] on the same materials (using the same fitting equation) in Table 1. In many cases, the fit parameters correlate to physical properties, and may sometimes be validated by comparison to independent estimates. For example, the adsorbent micropore volume can be determined by the Dubinin-Radushkevich method[33] and compared to V_{max}. Likewise the product of the adsorbent micropore volume and the liquid molar density of the adsorbate[37] (n_m) provides an estimate of n_{max}. Rigorous comparisons of the fitted and independently estimated parameters are shown in Table 2.

Table 1. Best-fit parameters from Generalized Langmuir Fits.

	n_{max} (mmol g^{-1})	α	V_{max} (mL g^{-1})	A_1 (k$^{1/2}$ MPa^{-1})	E_1 (kJ mol^{-1})	A_2 (k$^{1/2}$ MPa^{-1})	E_2 (kJ mol^{-1})
CO_2 /ZTC	45.4	1.64E^{-12}	12.4	0.00143	21.6	0.121	3.94
CO_2 /CNS-201	12.9	0.800	3.41	0.0456	23.0	0.00244	22.0
CO_2/MSC-30	81.1	0.207	10.0	0.000107	23.6	0.0635	14.3
CH_4/ZTC	35.6	0.460	2.04	0.0590	11.6	0.000180	20.4
CH_4/CNS-201	9.77	0.580	0.490	0.0610	17.2	0.00440	16.4
CH_4/MSC-30	41.0	0.700	2.30	0.0680	13.4	0.00460	12.9
C_2H_6/ZTC	25.0	0.827	1.58	2.14E-07	41.0	0.0444	18.5
C_2H_6/MSC-30	36.1	0.713	2.60	0.0865	19.8	0.00647	17.8
Kr/ZTC	39.3	0.686	2.02	1.81E-06	30	0.0924	10.0
Kr/CNS-201	10.9	0.462	0.490	0.00590	15.1	0.0689	16.3
Kr/MSC-30	57.8	0.726	2.98	0.112	11.6	0.00306	12.8

Table 2. Comparison of V_{max} and n_{max} Parameters to Independent Estimates

	V_{max} (mL g^{-1})	micropore volume (mL g^{-1})	n_{max} (mmol g^{-1})	n_m (mmol g^{-1})
CO_2 /ZTC	12.4	1.66	45.4	44.5
CO_2 /CNS-201	3.41	0.45	12.9	12
CO_2/MSC-30	10.0	1.54	81.1	41.3
CH_4/ZTC	2.04	1.66	35.6	46.6
CH_4/CNS-201	0.490	0.45	9.77	13
CH_4/MSC-30	2.30	1.54	41.0	43.3
C_2H_6/ZTC	1.58	1.66	25.0	36.0
C_2H_6/MSC-30	2.60	1.54	36.1	33.4
Kr/ZTC	2.02	1.66	39.3	48.5
Kr/CNS-201	0.490	0.45	10.9	13
Kr/MSC-30	2.98	1.54	57.8	45.0

Although more difficult to validate through independent comparison, the E_i parameters give important insight into the adsorbent-adsorbate binding energies of the i^{th} isotherm, and the prefactor A_i gives insight about the relative number of adsorption sites with energy E_i. Specifically, the product of α_i, the i^{th} isotherm weighting factor, and A_i gives an overall "weight" of sites with energy E_i. For carbon dioxide, methane, ethane and krypton adsorption on MSC-30 and CNS-201, the contributions of each isotherm in the fitted superposition of isotherms are moderately well-balanced. No isotherm accounts for less than 1% of the overall "weight", except for carbon dioxide on MSC-30. This may result from carbon dioxide adsorbing on a more limited set of MSC-30 adsorption sites than other gases, as noted on single-wall carbon nanotube bundles[42].

For ZTC, each generalized Langmuir fit heavily favors just a single isotherm (see Table 3). This suggests that ZTC usually has a higher degree of binding-site homogeneity than MSC-30 or CNS-201, consistent with the pore-size distributions of the three carbonaceous adsorbents. Unlike MSC-30 and CNS-201, ZTC has a single sharply peaked pore width (1.2

nm). In microporous carbons, the predominant contribution to binding-site heterogeneity often results from the spectrum of pore widths. ZTC eliminates much of this heterogeneity with its micropores of approximately a constant width.

Table 3. Normalized Relative Weights of Isotherms 1 and 2 as Determined by Multiplying the Isotherm Weighting Value (α_i) by the Isotherm Prefactor ($\mathcal{A}_i$)

	Isotherm 1 Weight	Isotherm 2 Weight
CO_2 /ZTC	1.94E-14	1.00E+00
CO_2 /CNS-201	9.87E-01	1.32E-02
CO_2/MSC-30	4.40E-04	1.00E+00
CH_4/ZTC	9.96E-01	3.57E-03
CH_4/CNS-201	9.50E-01	4.96E-02
CH_4/MSC-30	9.72E-01	2.82E-02
C_2H_6/ZTC	2.30E-05	1.00E+00
C_2H_6/MSC-30	9.71E-01	2.92E-02
Kr/ZTC	4.28E-05	1.00E+00
Kr/CNS-201	6.85E-02	9.32E-01
Kr/MSC-30	9.90E-01	1.02E-02

The Clapeyron relation was used to determine the isosteric heat of adsorption:

$$q_{st} = -\Delta H_{ads}(n_a) = -T\left(\frac{\partial P}{\partial T}\right)_{n_a}(\Delta v_{ads}) \quad (5)$$

Here the isosteric heat of adsorption (q_{st}) is (by convention) a positive value when adsorption is exothermic. The coverage-dependent change in enthalpy upon adsorption is $\Delta H_{ads}(n_a)$. The change in molar volume of the adsorbate upon adsorption is Δv_{ads}.

4. Discussion

4.1. Isosteric Heat of Carbon Dioxide Adsorption

The isosteric heats of carbon dioxide adsorption on MSC-30, CNS-201, and ZTC derived according to Equation 5 are shown in Figure 3. The isosteric heat of carbon dioxide adsorption on MSC-30 differs significantly from that on a conventional activated carbon like CNS-201 in its dependence on absolute uptake. For carbon dioxide adsorption on CNS-201, the isosteric heat displays typical behavior. It is a decreasing function of occupancy. On the other hand, the isosteric heat of carbon dioxide adsorption on MSC-30 first increases as a function of occupancy before reaching a maximum, and then decreases at high occupancy. On ZTC, the isosteric heat of carbon dioxide adsorption decreases very gradually with loading, especially at low temperatures where the slope is ~ -25kJ•mol^{-2}. This behavior is in agreement with the high degree of binding-site homogeneity expected from the pore-size distribution and fit parameters for ZTC. Carbon dioxide adsorption differs from methane, ethane, and krypton adsorption where the isosteric heats on MSC-30 decrease with occupancy, while the isosteric heats on ZTC increase with occupancy due to enhanced adsorbate-adsorbate interactions. This suggests that carbon dioxide adsorbate-adsorbate interactions are better optimized for the micropore distribution of MSC-30 than ZTC.

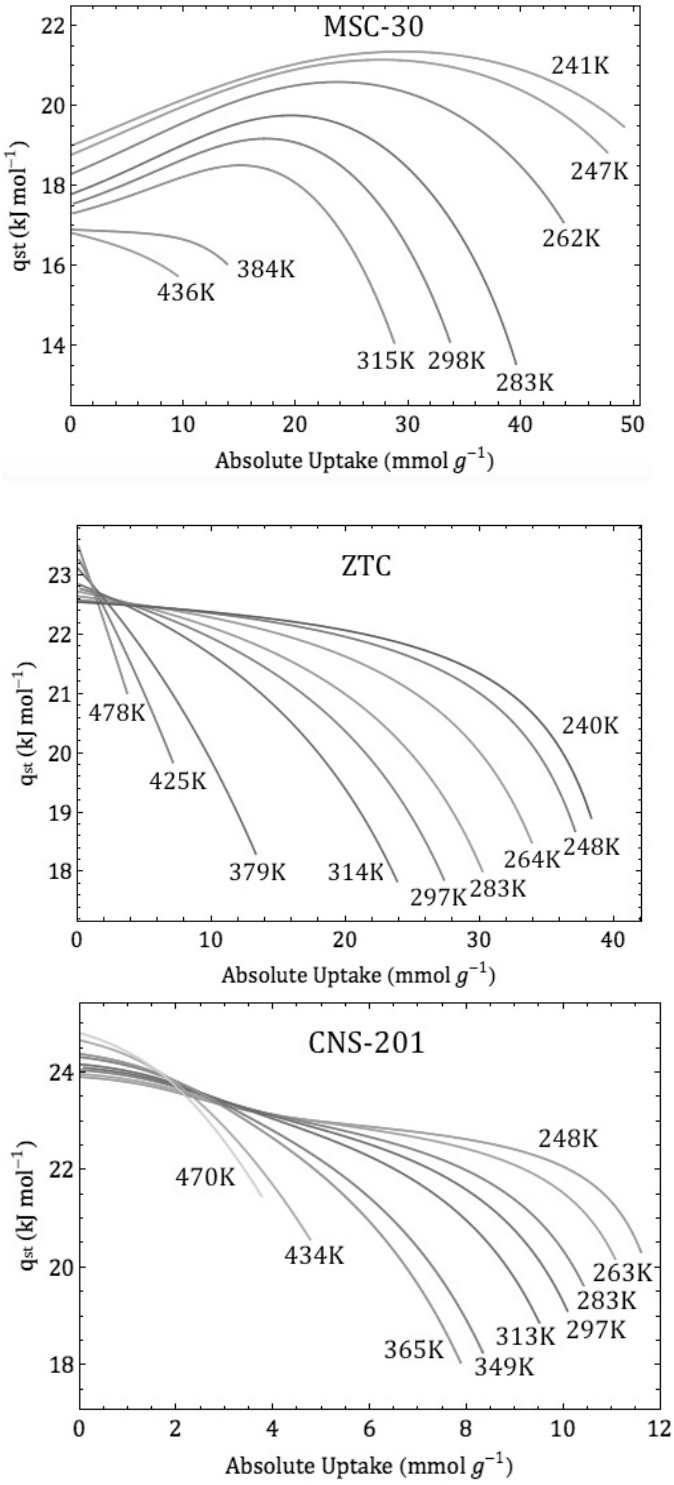

Figure 3. Isosteric heats of adsorption of carbon dioxide on CNS-201, MSC-30, and ZTC as a function of absolute uptake.

For carbon dioxide adsorbed on MSC-30, the total increase in isosteric heat (peak value minus low coverage value) is more pronounced at lower temperatures, reaching a maximum measured increase of 2.1 kJ•mol^{-1} at 241 K. This energy is consistent with lateral intermolecular interactions between adsorbed carbon dioxide molecules. For example, the well depth of the Lennard-Jones potential between two carbon dioxide molecules is ε = 1.8 kJ•mol^{-1} [43].

At low temperatures and low occupancy, the isosteric heat of adsorption of carbon dioxide on MSC-30 increases approximately linearly with occupancy. This linear increase is nearly identical for the lowest temperatures measured (e.g. 107 kJ•g•mol^{-2} at 241 K, 111 kJ•g•mol^{-2} at 247 K, 113 kJ•g•mol^{-2} at 262 K and 106 kJ•g•mol^{-2} at 283 K). Similar trends hold true for methane, ethane, and krypton adsorption on ZTC.[25,26,27] The gases with stronger intermolecular interactions have larger slopes, consistent with the hypothesis that the increases in the isosteric heats with loading result from adsorbate-adsorbate intermolecular interactions. The slopes of the isosteric heats with respect to fractional occupancy, $\frac{\partial(-\Delta H_{ads})}{\partial\theta}$, may be reasonably estimated with Equation 6 (see Table 4) in the low coverage regime

$$\frac{\partial(-\Delta H_{ads})}{\partial\theta} = \frac{z\varepsilon}{2} \qquad (6)$$

where the coordination number, z, is posited to be 5 and ε is the well depth of the Lennard-Jones 12-6 interaction potential[43]. This simple first approximation (Equation 6) assumes that adsorbed molecules are randomly situated and only interact with first nearest neighbors, each interaction having strength ε.

Table 4. Measured and Estimated Slopes of Increasing Isosteric Heats of Methane, Ethane, and Krypton on ZTC, and Carbon Dioxide on MSC-30 as a Function of Fractional Occupancy (at Low Coverage and Low Temperature)

	Estimated Slope (kJ•mol^{-1})	Measured Slope (kJ•mol^{-1})
Methane	3.0	3.2
Krypton	3.3	3.4
Ethane	4.3	4.0
Carbon Dioxide	4.5	4.5

A qualitatively similar increase in the isosteric heat of carbon dioxide adsorption on Maxsorb® (from Kansai Netsu Kagaku Co.) was previously noted by Himeno et al.[44], however it is unclear to what degree those results are quantitatively accurate. Himeno et al. used the Toth equation to fit three experimental isotherms (at 273, 298, and 323K). This fit was then used to calculate an isosteric heat via a reduced form of the Clausius-Clapeyron Equation (Equation 7).

$$\frac{\Delta H}{RT^2} = \left[\frac{\partial lnP}{\partial T}\right]_N \qquad (7)$$

The calculated "isosteric heat" (ΔH) was determined from the partial derivative of the logarithm of the pressure with respect to temperature at constant coverage (N). In this case, however, excess adsorption, not absolute adsorption was held constant and what was calculated may more aptly be called an "isoexcess heat of adsorption". At low coverage, excess adsorption accurately approximates absolute adsorption, but deviations arise and become significant as the equilibrium gas-phase density increases. In our work we employ a generalized Langmuir-type fitting function that determines absolute adsorption and gives true "isosteric

heats of adsorption". We have elaborated on this methodology in prior publications[25,26,27,29]. Additionally, Equation 7, which is employed by Himeno et al. but not in our work, makes two idealized assumptions that break down for nonideal gas conditions. Equation 7 assumes that the volume of the adsorbed phase is zero, and further assumes the validity of the ideal gas law. These assumptions lead to significant errors under nonideal gas conditions. Futhermore, our analysis determines the temperature dependence of the isosteric heat, which is ignored by Himeno et al. Himeno et al. report an increasing isosteric heat for carbon dioxide adsorption on Maxsorb® with a slope of ~300 ($kJ \bullet g \bullet mol^{-2}$). We report a more moderate slope (~110 $kJ \bullet g \bullet mol^{-2}$) on the comparable superactivated carbon MSC-30 after considering isotherms taken at eight temperatures. This more moderate increase is more consistent with the strength of carbon dioxide intermolecular interactions as measured by the Lennard-Jones parameter, ε=1.8 kJ/mol[43], Equation 6 and the trend in Table 3.

4.2 Adsorbed-Phase Enthalpies and Heat Capacities

The adsorbed-phase enthalpies for carbon dioxide adsorption on MSC-30, CNS-201, and ZTC were calculated as a function of absolute adsorption by subtracting the isosteric heats in Figure 3 from gas-phase enthalpy values determined from data tables at equivalent conditions[37]. Figure 4 shows that MSC-30 has different behavior than CNS-201 or ZTC in that the adsorbed-phase enthalpy is not a monotonically increasing function of coverage. Rather the adsorbed-phase enthalpy on MSC-30 decreases with coverage at low temperatures and low coverages, consistent with enhanced favorable adsorbate-adsorbate interactions.

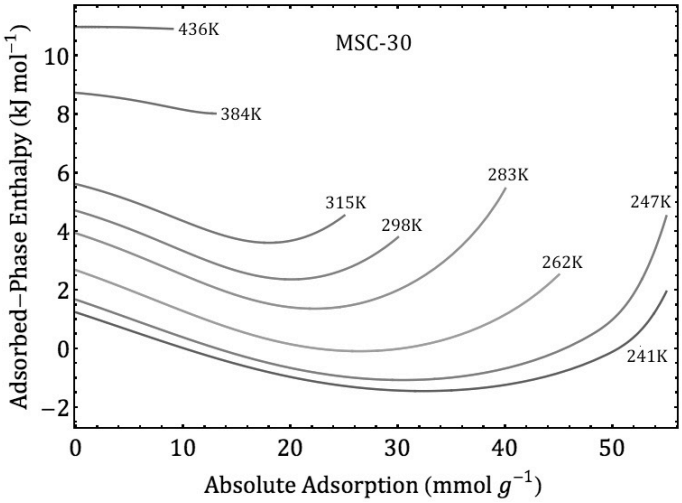

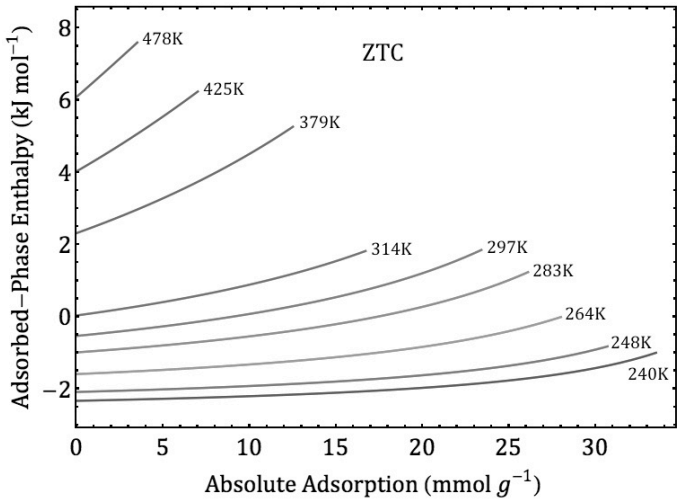

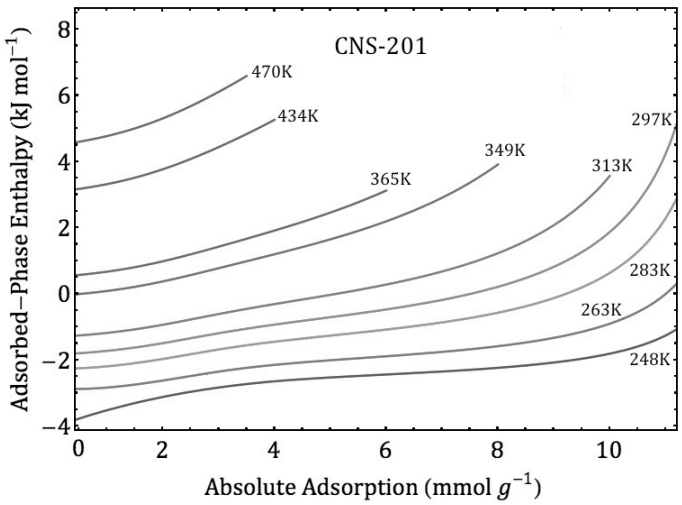

Figure 4. Adsorbed-phase enthalpies of carbon dioxide on MSC-30, ZTC, and CNS-201.

The adsorbed-phase constant pressure heat capacities of carbon dioxide on MSC-30, CNS-201, and ZTC were calculated by taking the partial derivative of the adsorbed-phase enthalpies with respect to temperature at constant pressure. Figure 5 shows the adsorbed-phase heat capacities at a constant sample pressure of 2 MPa.

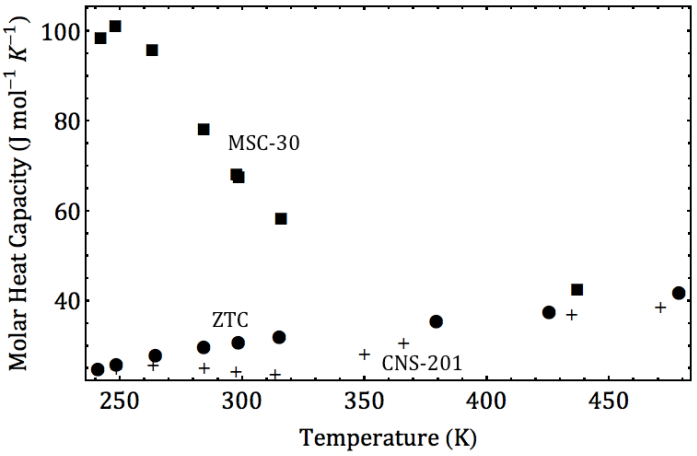

Figure 5. Adsorbed-phase molar heat capacities of carbon dioxide on MSC-30 (■), CNS-201 (+), and ZTC (•). Values are given at a constant sample pressure of 2 MPa.

Figure 5 shows that the constant pressure adsorbed-phase heat capacities of carbon dioxide on CNS-201 and ZTC gradually increase with temperature as expected for a polyatomic gas. On MSC-30 a different behavior is observed where the adsorbed-phase heat capacity rises significantly around a temperature of 250K. This is suggestive of a phase transition and indicates that the origin of the enhanced adsorbate-adsorbate interactions may be an adsorbed-phase clustering transition as previously noted in other systems.[29,30]

4.3 Law of Corresponding States and Selectivities

It is well established that different nonideal gases behave similarly at corresponding conditions, at equal reduced temperatures and reduced pressures.[45] The reduced temperature and reduced pressure are defined as the ratios of the system temperature to the gas critical temperature, and the system pressure to the gas critical pressure, respectively. We have recently reported an extension to the Law of Corresponding States that applies to physisorbed molecules.[30] Specifically:

Classical gases adsorb to the same fractional occupancy on the same adsorbent at corresponding conditions.

Fractional occupancy (θ) is defined as the ratio of the absolute adsorption (n_a) to maximum possible adsorption (n_m). To facilitate comparisons in this work and others,[30] we instead compare the more accessible quantity, excess occupancy (θ_e), defined as the ratio of excess adsorption (n_e) to maximum possible adsorption (n_m). For each adsorbent, n_m was estimated by multiplying the adsorbent micropore volume by the liquid molar density of the adsorbate at its triple point.[30,37] Carbon dioxide, ethane, methane, and krypton excess occupancy isotherms on ZTC and MSC-30 are compared at corresponding conditions in Figure 6.

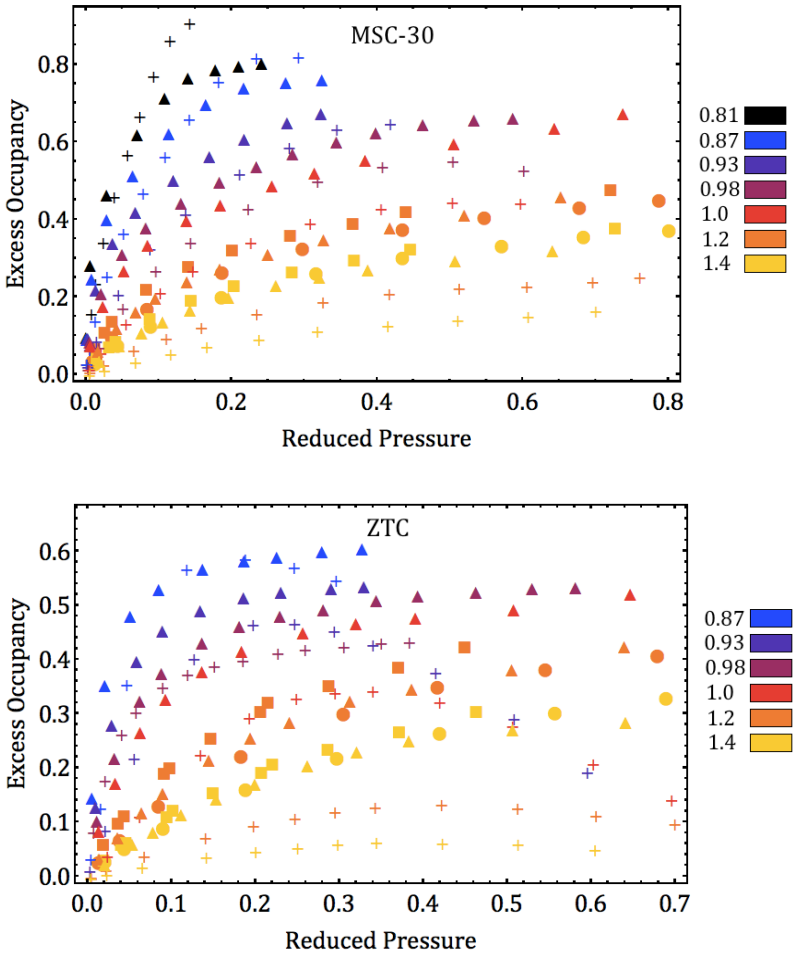

Figure 6. Comparison of carbon dioxide (+), ethane (Δ), methane (■), and krypton (•) excess occupancies at corresponding conditions (with reduced temperatures given in the key).

At low temperatures, there is reasonable agreement between carbon dioxide and ethane isotherms at corresponding conditions. At higher temperatures, however, the carbon dioxide isotherms are significantly smaller than corresponding isotherms of the other gases. This may be due in part to the large quadrupole moment of carbon dioxide[46], which is not present in the other gases considered. The large quadrupole moment accounts for ~50% of the cohesive energy of solid carbon dioxide.[47,48] Notably the bulk critical temperature and isosteric heats of carbon dioxide and ethane are similar in spite of carbon dioxide's significantly

lower polarizability. This is also consistent with a strong quadrupole interaction of carbon dioxide.[49,50,51] It is possible that the short-range quadrupole-induced dipole interactions between carbon dioxide and the adsorbent are disrupted with temperature, but further investigation is needed.

The selectivities of carbon dioxide with respect to methane, ethane and krypton were calculated as the ratio of the Henry's Law constants. Henry's Law constants were calculated directly from the excess adsorption data by extrapolating to zero coverage the logarithm of pressure divided by excess adsorption ($\ln(P/n_e)$).[52] The measured room temperature Henry's Law constants and selectivities are given in Table 5. Methane and krypton have similar Henry's Law constants, as one might expect based on the similarity of the gases, particularly their similar critical temperatures. While carbon dioxide and ethane have nearly identical critical temperatures, ethane has significantly higher room temperature Henry's Law constants for each adsorbent. This is consistent with the trends noted in Figure 6.

Table 5. Henry's Law Constants (mmol g^{-1} MPa^{-1}) and Equilibrium Adsorption Selectivities at Room Temperature

Henry's Law Constants	ZTC	MSC-30	CNS-201
C_2H_6	45.7	51.9	35.1
CO_2	19.7	19.9	21.4
CH_4	7.03	8.99	6.99
Kr	6.80	9.03	6.57
CO_2/CH_4	2.80	2.21	3.06
C_2H_6/CO_2	2.32	2.61	1.64
CO_2/Kr	2.90	2.20	3.26
C_2H_6/CH_4	6.50	5.77	5.02
C_2H_6/Kr	6.72	5.75	5.34

5. Conclusions

The excess uptakes of carbon dioxide on MSC-30, CNS-201, and ZTC were measured volumetrically and fitted with a generalized Langmuir-type equation. The fitted data were used in thermodynamic analyses that show how MSC-30 exhibits an atypical, increasing isosteric heat of carbon dioxide adsorption, while CNS-201 has the thermodynamic properties of a conventional carbon. The isosteric heat on ZTC suggests a high degree of binding-site homogeneity. At near-ambient temperatures the isosteric heat on MSC-30 rises with uptake from 19 to 21 $kJ \bullet mol^{-1}$. The measured adsorbed-phase enthalpies, adsorbed-phase heat capacities, and comparisons to studies with other nonideal gases indicate that this increasing isosteric heat results from enhanced adsorbate-adsorbate interactions within the pores of MSC-30.

Acknowledgements

This work was supported as part of EFree, an Energy Frontier Research Center under Award No. DE-SC0001057. A special thanks to Christopher Gardner for his contributions in the lab.

References:

1. Climate change 2013: The physical science basis. Intergovernmental Panel on Climate Change, Ed. Cambridge: Cambridge University Press, 2014.
2. Haszeldine RS. Carbon capture and storage: How green can black be? Science 2009; 325: 1647-1652.
3. Boot-Handford ME, Abanades JC, Anthony EJ, et al. Carbon capture and storage update. Energy Environ Sci. 2014; 7: 130-189.
4. Ruthven DM. Principles of Adsorption and Adsorption Processes. New York: Wiley, 1984.
5. Sircar S. Basic research needs for design of adsorptive gas separation processes. Ind Eng Chem Res. 2006; 45: 5435-5448.
6. Tedds S, Walton A, Broom DP, Book D. Characterization of porous hydrogen storage materials: Carbons, zeolites, MOFs and PIMs. Faraday Discuss. 2011; 151: 75-94.
7. Matranga KR, Myers AL, Glandt ED. Storage of natural-gas by adsorpiton on activated carbon. Chem Eng Sci. 1992; 47: 1569-1579.
8. Jasra RV, Choudary NV, Bhat SGT. Separation of gases by pressure swing adsorption. Separ Sci and Technol. 1991; 26: 885-930.
9. Sircar S, Golden TC, Rao MB. Activated carbon for gas separation and storage. Carbon. 1996; 34: 1-12.
10. Choi S, Drese JH, Jones CW. Adsorbent materials for carbon dioxide capture from large anthropogenic point sources. Chem Sus Chem. 2009; 2: 796-854.
11. D'Alessandro DM, Smit B, Long JR. Carbon dioxide capture: Prospects for new materials. Angew Chem Int Ed. 2010; 49: 6058-6082.
12. Chen ZH, Deng SB, Wei HR, Wang B, Huang J, Yu G. Activated carbons and amine-modified materials for carbon dioxide capture – A review. Front Environ Sci Eng. 2013; 7: 326-340.
13. Sircar S, Mohr R, Ristic C, Rao MB. Isosteric heat of adsorption: Theory and experiment. J Phys Chem B. 1999; 103: 6539-6546.
14. Bhatia SK, Myers AL. Optimum conditions for adsorptive storage. Langmuir. 2006; 22: 1688-1700.
15. Simon CM, Kim J, Lin LC, Martin RL, Haranczyk M, Smit B. Optimizing nanoporous materials for gas storage. Phys Chem Chem Phys. 2014; 16: 5499-5513.
16. Lee SY, Park SJ. Determination of the optimal pore size for improved CO2 adsorption in activated carbon fibers. J Colloid Interface Sci. 2013; 389: 230-235.
17. Gargiulo N, Pepe F, Caputo D. CO2 adsorption by functionalized nanoporous materials: A review. J Nanosci Nanotechnol. 2014; 14: 1811-1822.
18. Bae YS. Snurr RQ. Development and evaluation of porous materials for carbon dioxide separation and capture. Angew Chem Int Ed. 2011; 50: 11586-11596.
19. Furukawa H, Yaghi OM. Storage of hydrogen, methane, and carbon dioxide in highly porous covalent organic frameworks for clean energy applications. J Am Chem Soc. 2009; 131: 8875– 8883.

20. Wang QA, Luo JZ, Zhong ZY, Borgna A. CO2 capture by solid adsorbents and their applications: current status and new trends. Energy Environ Sci. 2011; 4: 42-45.
21. Wang B, Cote AP, Furukawa H, O'Keeffe M, Yaghi OM. Colossal cages in zeolitic imidazolate frameworks as selective carbon dioxide reservoirs. Nature. 2008; 453: 207-211.
22. Simmons JM, Wu H, Zhou W, Yildirim T. Carbon capture in metal-organic frameworks – A comparative study. Energy Environ Sci. 2011; 4: 2177-2185.
23. Zhou J, Li W, Zhang ZS, Xing W, Zhuo SP. Carbon dioxide adsorption performance of N-doped zeolite Y templated carbons. RSC Adv. 2012; 2: 161-167.
24. Al-Muhtaseb SA, Ritter JA. Roles of surface heterogeneity and lateral interactions on the isosteric heat of adsorption and adsorbed phase heat capacity. J Phys Chem B. 1999; 103: 2467-2479.
25. Stadie NP, Murialdo M, Ahn CC, Fultz B. Anomalous isosteric enthalpy of adsorption of methane on zeolite-templated carbon. J Am Chem Soc. 2013; 135: 990-993.
26. Murialdo M, Stadie NP, Ahn CC, Fultz B. Observation and investigation of increasing isosteric heat of adsorption of ethane on zeolite-templated carbon. J Phys Chem C. 2015; 119: 944-950.
27. Murialdo M, Stadie NP, Ahn CC, Fultz B. Krypton adsorption on zeolite-templated carbon and anomalous surface thermodynamics. Langmuir. 2015; 31: 7991-7998.
28. Mu B, Walton KS. High-pressure adsorption equilibrium of CO2, CH4, and CO on an impregnated activated carbon. J Chem Eng Data. 2011; 56: 390-397.
29. Stadie NP, Murialdo M, Ahn CC, Fultz B. Unusual entropy of adsorbed methane on zeolite-templated carbon. J Phys Chem C. 2015; 119: 26409-26421.
30. Murialdo M, Stadie NP, Ahn CC, Fultz B. A generalized law of corresponding states for the physisorption of classical gases with cooperative adsorbate-adsorbate interactions. J Phys Chem C. 2016; 120: 11847-11853.
31. Nishihara H, Hou PX, Li LX, et al. High-pressure hydrogen storage in zeolite-templated carbon. J Phys Chem C. 2009; 113: 3189-3196.
32. Brunauer S, Emmett PH, Teller E. Adsorption of gases in multimolecular layers. J Am Chem Soc. 1938; 60: 309-319.
33. Nguyen C, Do DD. The Dubinin-Radushkevich equation and the underlying microscopic adsorption description. Carbon. 2001; 39: 1327-1336.
34. Rouquerol J, Rouquerol F, Llewellyn P, Maurin G, King KSW. Adsorption by powders and porous solids: Principles, methodology and applications. 2nd ed. Oxford: Academic Press, 2014.
35. Tarazona P, Marconi UMB, Evans R. Phase-equilibria of fluid interfaces and confined fluids-nonlocal versus local density functionals. Mol Phys. 1987; 60: 573–595.
36. Bowman RC, Luo CH, Ahn CC, Witham CK, Fultz B. The effect of tin on the degradation of LaNi5-ySny metal-hydrides during thermal cycling. J Alloys Compd. 1995; 217: 185-192.

37. Lemmon, E. W.; Huber, M. L.; McLinden, M. O. NIST Standard Reference Database 23: Reference Fluid Thermodynamic and Transport Properties, version 8.0; National Institute of Standards and Technology: Gaithersburg, MD, 2007; CD-ROM.
38. Stadie NP, Vajo JJ, Cumberland RW, Wilson AA, Ahn CC, Fultz B. Zeolite-templated carbon materials for high-pressure hydrogen storage. Langmuir. 2012; 28: 10057-10063.
39. Youn HK, Kim J, Chandrasekar G, Jin H, Ahn WS. High pressure carbon dioxide adsorption on nanoporous carbons prepared by zeolite Y templating. Mater Lett. 2011; 65: 1772-1774.
40. Sircar S. Gibbsian surface excess for gas adsorption-Revisited. Ind Eng Chem Res. 1999; 38: 3670-3682.
41. Mertens FO. Determination of absolute adsorption in highly ordered porous media. Surf Sci. 2009; 603: 1979-1984.
42. Bienfait M, Zeppenfeld P, Dupont-Pavlovsky N, et al. Thermodynamics and structure of hydrogen, methane, argon, oxygen, and carbon dioxide adsorbed on single-wall carbon nanotube bundles. Phys Rev B. 2004; 70: 035410(1-10).
43. Tee LS, Gotoh S, Stewart WE. Molecular parameters for normal fluids - Lennard-Jones 12-6 potential. Ind Eng Chem Fundam. 1966; 5: 356-363.
44. Himeno S, Komatsu T, Fujita S. High-pressure adsorption equilibria of methane and carbon dioxide on several activated carbons. J Chem Eng Data. 2005; 50: 369-376.
45. Guggenheim EA. The principle of corresponding states. J Chem Phys. 1945; 13: 253-261.
46. Graham C, Pierrus J, Raab RE. Measurement of the electric quadrupole-moments of CO2, CO and N2. Mol Phys. 1989; 67: 939-955.
47. Slusarev VA, Freiman YA, Krupskii IN, Burakhov IA. Orientational Disordering and Thermodynamic Properties of Simple Molecular-Crystals. Phys Status Solidi B. 1972; 54: 745-754.
48. Hirshfeld FL, Mirsky K. Electrostatic term in lattice-energy calculations - C2H2, CO2, AND C2N2. Acta Crystallogr Sect A. 1979; 35: 366-370.
49. Buckingham AD, Disch RL. Quadrupole moment of carbon dioxide molecule. Proc R Soc A. 1963; 273: 275-289.
50. Do DD, Do HD. Effects of potential models on the adsorption of carbon dioxide on graphitized thermal carbon black: GCMC computer simulations. Colloids Surf A. 2006; 277: 239-248.
51. Terlain A, Larher Y. Phase-diagrams of films of linear-molecules with large quadrupole-moments (CO2, N2O, C2N2) adsorbed on graphite. Surf Sci. 1983; 125: 304-311.
52. Zhang SY, Talu O, Hayhurst DT. High-pressure adsorption of methane in NaX, MgX, CaX, SrX, and BaX. J Phys Chem. 1991; 95: 1722-1726.